Proceedings of the 4th International Conference on Functional Materials and Civil Engineering
DOI: 10.54254/2755-2721/2026.36782

Interface Challenges and Engineering Strategies in Sulfide Solid Electrolyte-Based All-Solid-State Lithium–Sulfur Batteries

Liangyu Li

Department of Chemical and Environmental Engineering, The University of Nottingham Ningbo China, Ningbo, China
ssyll7@nottingham.edu.cn

Abstract. All-solid-state lithium–sulfur batteries (ASSLSBs) combine sulfur's theoretical specific capacity of 1675 mA h g^{-1} with the safety potential of nonvolatile solid electrolytes. By eliminating the liquid dissolution–diffusion medium, sulfide solid electrolytes (sulfide SSEs) suppress conventional polysulfide migration while retaining high room-temperature Li-ion conductivity and favorable processability. This replacement, however, converts a liquid-wetted porous electrode into a pressed solid assembly in which sulfur conversion depends on real contact and coupled ion/electron transport. Chemical failure arises from sluggish S_8/Li_2S conversion and oxidative or reductive decomposition of sulfide SSEs, whereas physical failure arises from dynamic three-phase-contact loss, conversion strain, through-thickness reaction gradients, stripping voids, and lithium penetration. This focused perspective examines selected primary studies through an evidence-normalization lens, distinguishing direct observations from cross-study inference under explicit capacity bases and test boundaries. Across these studies, stable cycling is associated with selective interfacial chemistry, continuous ionic/electronic pathways, and sustainable mechanical contact; neither high bulk ionic conductivity nor high stack pressure alone removes interfacial failure. Practical comparisons should report loading, current, temperature, pressure, electrolyte thickness, and inactive-component inventory together with gravimetric performance. This perspective separates mechanistic evidence from metrics inflated by low loading, elevated temperature, or reversible non-sulfur charge storage.

Keywords: All-Solid-State Lithium–Sulfur Batteries, Sulfide Solid Electrolytes, Solid–Solid Interfaces, Interface Failure Mechanisms

1. Introduction

Lithium–sulfur chemistry stores charge through a multielectron conversion reaction and offers a theoretical sulfur capacity of 1675 mAh g^{-1}. The active-material value is attractive, but practical energy density also depends on the electrolyte, conductive additive, separator, current collectors, and lithium inventory. Conventional liquid cells additionally suffer from dissolution and migration of polysulfides, electrolyte consumption, and an unstable lithium surface. Consequently, improvements

© 2026 The Authors. This is an open access article distributed under the terms of the Creative Commons Attribution License 4.0 (https://creativecommons.org/licenses/by/4.0/).

DOI: 10.54254/2755-2721/2026.36782

observed at low sulfur loading or with large excesses of electrolyte and lithium cannot be translated directly into cell-level specific energy [1, 2]. A sulfur-mass-normalized capacity can remain high even when inactive components dominate cell mass or short transport distances conceal electrode-scale limitations.

ASSLSBs replace the liquid phase with a solid ion conductor. The absence of a liquid solvent suppresses the conventional dissolution–diffusion shuttle, while many sulfide SSEs provide predominantly Li-ion conduction, high room-temperature conductivity, and sufficient compliance for cold pressing. These advantages create a different limitation: a solid cannot flow to restore contact after S_8/Li_2S conversion or lithium stripping. The composite cathode must therefore maintain continuous ionic and electronic networks and stable three-phase contact, while both the carbon/sulfide-SSE and lithium/sulfide-SSE interfaces remain susceptible to electrochemical decomposition [1, 2]. Pressability helps densify particle contacts and reduce electrolyte thickness, but it does not prevent oxidation at carbon-rich cathodes, reduction at lithium, or void formation during cycling.

Rather than providing an exhaustive survey, this focused perspective examines a selected set of illustrative primary studies. Section 2 links working principles to coupled chemical and physical failure; Section 3 evaluates targeted engineering strategies under comparable operating boundaries. Because mediators and reversible electrolyte reactions can also store charge, apparent capacity is not automatically equivalent to sulfur utilization. Where available, capacity normalization and relevant temperature, current, loading, pressure, or anode boundaries are stated explicitly.

2. Working principles, cell architecture, and interface challenges

2.1. Working principles

A typical ASSLSB contains an S_8 or Li_2S composite cathode, a dense sulfide-SSE layer, and a lithium-containing anode. During discharge, lithium ions and electrons reach the cathode through separate pathways and drive the overall solid-state conversion; charging reverses the reaction.

Solid-state conversion is not strictly one-step. Operando and ex situ measurements identify metastable Li_2S_2 and residual S_8/Li_2S_2 even after nominal full lithiation [3]. These residual phases show that practical utilization is controlled by interfacial transport and local reaction accessibility, not by thermodynamic capacity alone. The solid environment limits long-range redistribution, so local pathway interruption can leave chemically recoverable sulfur isolated from either ions or electrons.

2.2. Cell architecture

The cell is a three-layer stack consisting of the composite cathode, dense solid-electrolyte layer, and anode. The electrolyte layer carries Li^+ through the thickness while electronically isolating the electrodes. Its two boundaries experience different reaction environments: the cathode side is driven toward oxidation, whereas the lithium side is driven toward reduction.

Within the cathode, active material, conductive carbon, and sulfide SSE form effective reaction zones rather than a fixed geometric line. The effective reaction front migrates and the local triple-phase-boundary (TPB) network is continuously reconstructed during S_8/Li_2S conversion, volume change, and interfacial decomposition. Mixed-conducting interphases may broaden the effective zone beyond a strict geometric TPB, but stable operation still requires both networks and their contact topology to remain connected.

DOI: 10.54254/2755-2721/2026.36782

2.3. Interface challenges

2.3.1. Chemical challenges

The first chemical limitation is the low electronic conductivity of sulfur species and the restricted solid-state transport of reaction intermediates. In the modified Bruggeman relation used by Ohno et al. [4], the fitted tortuosity-factor–electrolyte-volume-fraction relationship gave $\gamma = 1.53$ and $\beta = 6.97$, compared with $\beta = 0.5$ for the original spherical-inclusion Bruggeman case. Here β is the exponent governing how rapidly effective ionic conductivity falls as the electrolyte volume fraction decreases; the unusually high value indicates strong microstructural sensitivity and a large fraction of ionically isolated electrolyte, not a direct measurement of tortuosity. Consequently, selecting an SSE with higher bulk conductivity does not ensure high effective conductivity when mixing and percolation isolate a substantial fraction of the ionic phase.

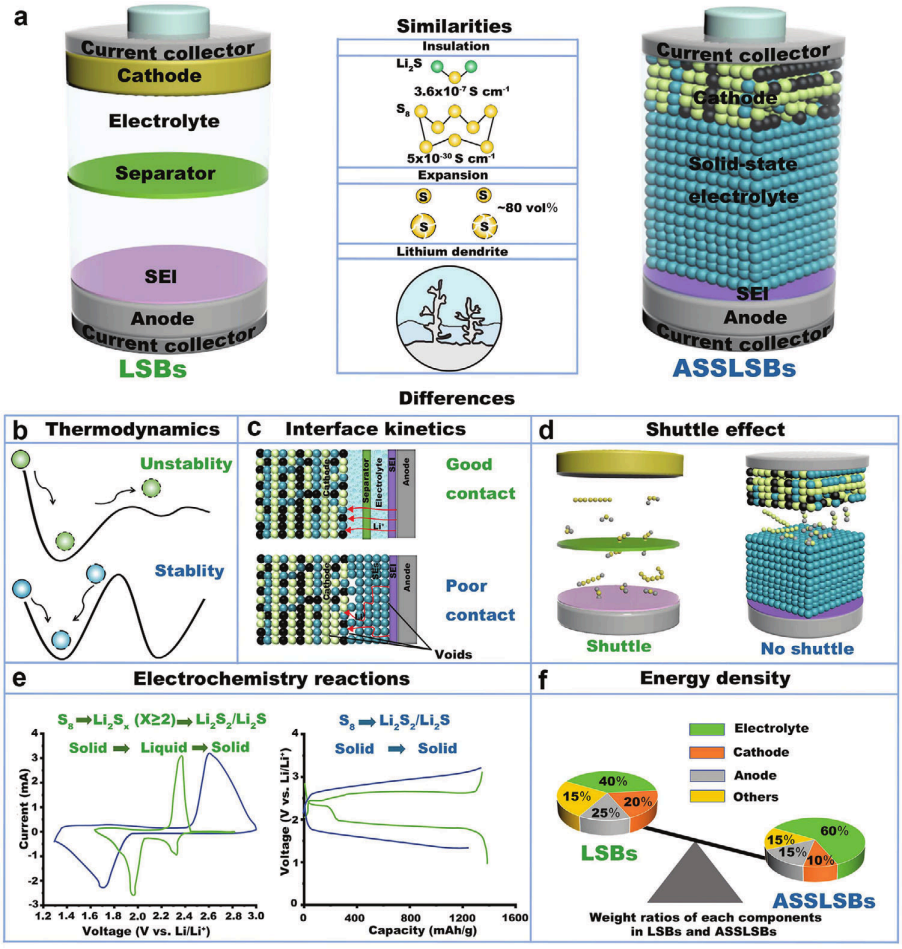

Figure 1. Reaction environment and interface differences between liquid and sulfide all-solid-state lithium–sulfur batteries. The source label "No shuttle" denotes suppression of the conventional liquid-phase dissolution–diffusion shuttle, not the absence of all side reactions or defect-mediated transport (reproduced from [1])

The second limitation is the finite electrochemical stability of sulfide SSEs. Carbon-assisted oxidation can form resistive cathode-side products, whereas lithium reduces $Li_{10}GeP_2S_{12}$-type (LGPS-type) electrolytes toward Li_2S, Li_3P, and Li–Ge alloy species; Li_3PS_4-type electrolytes

DOI: 10.54254/2755-2721/2026.36782

instead yield Li_2S and $Li_{3-x}P$-related products [1, 2]. A thin, uniform, Li^+-conducting and electron-blocking interphase may be self-limiting, but a thick, electronically leaky, or ion-blocking layer continuously consumes electrolyte and raises impedance. Because product chemistry depends on the sulfide framework, potential, and reaction state, a single decomposition-product list cannot be transferred across all SSEs. These interface constraints distinguish the solid-state reaction environment from that of a liquid Li–S cell, as summarized in Figure 1.

2.3.2. Physical challenges

Physical failure begins with particle-scale contact loss. Fan et al. [5] reported 1138 and 531 mAh g^{-1} on the Li_2S-mass basis after 30 cycles for nano-Li_2S paired with nano- and micrometer-scale Li_3PS_4, respectively. This comparison associates electrolyte particle-scale matching with improved contact retention, although it does not alone establish a universal causal relation. The approximately 78% theoretical expansion for $S_8 \rightarrow Li_2S$, estimated from reaction stoichiometry and phase densities [6], can further generate pores, cracks, and inactive regions. Surviving contacts then carry higher local current, amplifying polarization and making initially small defects electrochemically consequential.

Through-thickness reaction gradients form a separate limitation. Operando X-ray computed tomography showed nearly uniform reaction at 0.1C but increasing localization on the side adjacent to the dense solid-electrolyte layer at 0.2C and above; effective ionic conductivity fell approximately threefold during charge, and the authors attributed persistent lithiated regions to irreversible Li_2S accumulation [6]. At the anode, insufficient externally applied stack pressure can permit stripping voids, whereas excessive pressure during deposition can promote defect-assisted lithium penetration [7, 8]. Taken together, these observations from different cell configurations suggest lower and upper pressure constraints, rather than a universal non-monotonic optimum.

Evidence across separate studies is consistent with—rather than yet directly demonstrating—a feedback between chemical and physical degradation: contact defects may intensify polarization and decomposition, whereas resistive products may redirect ion flux and stress. Capacity and impedance should therefore be cross-validated with spectroscopic, imaging, electrochemical, and mechanical evidence.

3. Engineering strategies

Strategies are grouped by their dominant chemical or physical failure target. Their performance is interpreted against three linked objectives: selective interfacial chemistry, continuous ionic/electronic pathways, and sustainable mechanical contact under explicit test boundaries.

3.1. Strategies for chemical challenges

3.1.1. Regulating li2s activation and solid-phase reaction pathways

Redox mediators can oxidize insulating Li_2S without requiring direct carbon contact at every particle. Lithium phenyl selenide (PhSeLi) raised first-charge Li_2S utilization from about 30% to 81.5%; a 4:1 Li_2S: PhSeLi cathode retained 615.9 mAh g^{-1} on the reported composite-cathode mass basis after 400 cycles at about 1 mg cm^{-2} and 0.2 A g^{-1} with $Li_7P_3S_{11}$ and an In–Li anode [9]. Because PhSeLi stores charge and the reported average Coulombic efficiency slightly exceeded 100%, capacity normalization, cut-off conditions, and parasitic cathode/electrolyte reactions must be considered. The result demonstrates mediator-assisted activation, not a direct one-to-one measure of

DOI: 10.54254/2755-2721/2026.36782

sulfur utilization. The corresponding cycling, impedance, rate, and polarization data are shown in Figure 2.

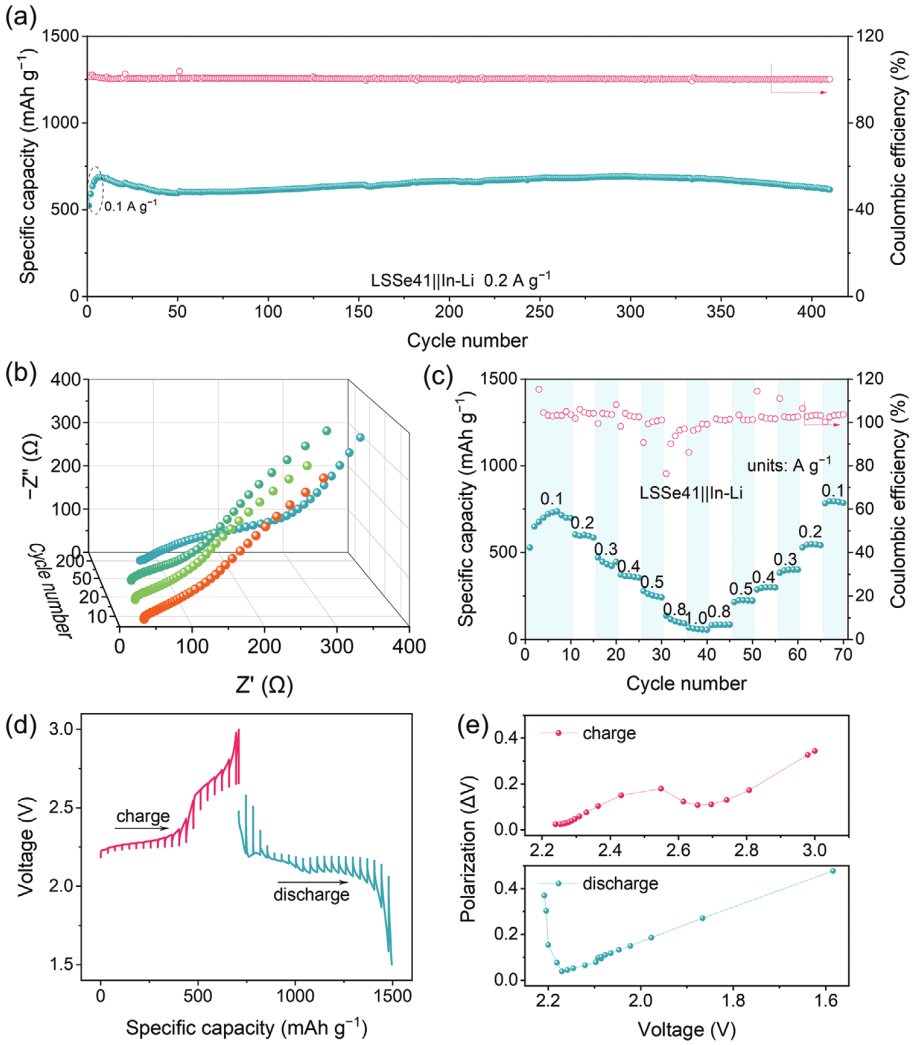

Figure 2. Long-term cycling, impedance, rate, and polarization data for the PhSeLi-mediated Li_2S cathode. Capacities use the composite-cathode mass basis reported by the authors; mediator and side-reaction contributions must be considered when interpreting sulfur utilization (reproduced from [9])

A particle-bound mediator can extend the reaction zone more selectively. $Li_2S/LiVS_2$ core–shell particles retained nearly 80% of their initial capacity over 1000 cycles at room temperature, 1 Ma cm^{-2}, and a moderate 2 mg cm^{-2} loading [10]. At 10 mg cm^{-2}, an areal capacity of 5.3 mAh cm^{-2} required 60 °C and had limited cycle life, so particle-level activation did not eliminate electrode-scale transport limits.

3.1.2. Constructing selective cathode-side interfaces

Iodide-based regulation illustrates how a reactive additive can both construct an interphase and carry charge. In a Li_2S–LiI–carbon/Li_3PS_4 cathode, LiI generated an amorphous Li–P–S–I interphase that persisted after discharge and was associated with reduced electrolyte decomposition [11]. Its thickness ranged from hundreds of nanometers to several micrometers in cells analyzed at 25 °C and

DOI: 10.54254/2755-2721/2026.36782

C/20 under operating stack pressures above 50 MPa; protection therefore does not imply that increasing thickness is beneficial, because thick regions lengthen ion-transport paths. A Li–B–P–S–I electrolyte using the $I^-/I_2/I_3^-$ couple delivered a charge capacity of 1497 mAh g^{-1} on a sulfur-mass basis at 2C and 30 °C, and retained 80.2% of its capacity after 25000 cycles at 5C and 25 °C [12]. Because the electrolyte is intentionally redox-active, sulfur-free controls are needed to separate its charge contribution.

Selective cathode-side interfaces can instead suppress decomposition. Kim et al. [13] formed an inorganic Li^+-conducting interphase at the S_8/Li_6PS_5Cl boundary and maintained 5.1 mAh cm^{-2} for 250 cycles at room temperature and 1 mA cm^{-2} using a sulfur loading of 4 mg cm^{-2}. Yu et al. [14] tuned a carbon-nitride/nitrogen-doped-graphene host to suppress oxidation of $Li_{5.5}PS_{4.5}Cl_{1.5}$ ($LPSCl_{1.5}$) and cycled a 2 mAh cm^{-2} cathode for more than 230 cycles. These mechanisms differ, and neither result implies that thicker interphases or simply less carbon will monotonically improve stability.

3.1.3. Stabilizing the lithium-anode/aulfide-electrolyte interface

Anode protection likewise requires Li^+ transport with electronic blocking. A chemically deposited Li_2S interphase on LGPS allowed Li/LGPS symmetric cells to operate for more than 500 h at 0.15 mA cm^{-2} [15]. The appropriate description is a Li^+-conducting, electron-blocking Li_2S interphase; symmetric-cell stability alone does not establish full-cell energy or capacity gains.

Bulk and interfacial design can be combined: a lithium-rich 80LiB alloy skeleton accommodates lithium-volume changes, while a silver-decorated carbon (Ag@C) layer homogenizes dissolution and deposition [16]. The full cell retained 82% of its capacity after 60 cycles, but this limited duration supports a mechanism-consistent interpretation rather than a general causal claim, and both B and Ag add inactive mass.

3.2. Strategies for physical challenges

3.2.1. Constructing bicontinuous networks and matching particle scales

Bicontinuous networks reduce the spatial mismatch between ionic and electronic pathways. Introducing amorphous Li_3PS_7 into ordered mesoporous carbon (CMK-3) placed ion conduction close to the sulfur/carbon network and retained 1025 mAh g^{-1} on the sulfur basis after 50 cycles at 60 °C and 1/8C with a lithium-metal anode [17]. The elevated temperature and inactive host/electrolyte mass limit direct cell-level comparison.

Particle-scale matching is likewise relevant. Nano-Li_2S with nano-Li_3PS_4 retained 1138 mAh g^{-1} after 30 cycles, whereas the micrometer-electrolyte combination retained 531 mAh g^{-1}, both on the Li_2S-mass basis [5]. Figure 3 compares the cycling and charge–discharge behavior of the three particle-size combinations. This comparison associates particle-scale matching with improved retention of ionic contact but does not prove that particle size is the only controlling variable. At higher loading, small mismatches can compound across electrode thickness and amplify contact-limited transport gradients.

DOI: 10.54254/2755-2721/2026.36782

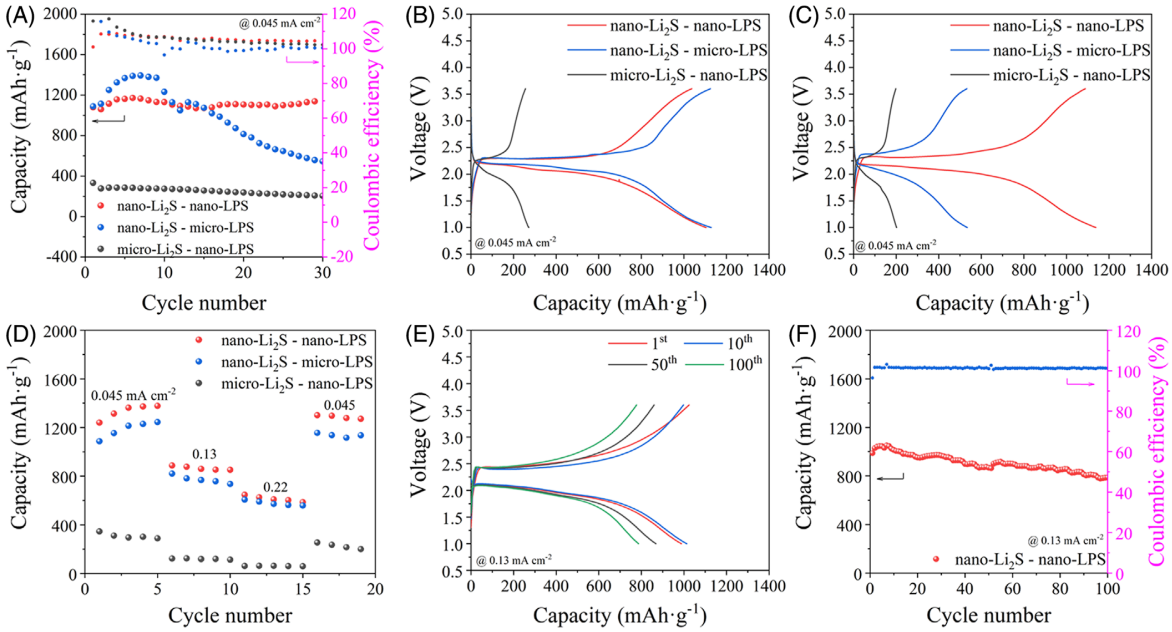

Figure 3. Cycling, rate, and charge–discharge behavior for Li_2S/Li_3PS_4 particle-size combinations. Cycling in panel (A) was measured at 0.045 mA cm^{-2}, and capacities are reported on the Li_2S-mass basis; the comparison associates matched nanoscale ionic contact with improved retention (reproduced from [5])

3.2.2. Opening ionic pathways inside high-loading cathodes

High-loading secondary particles can contain ionically inaccessible interiors. In situ conversion of a precursor into Li_3PS_4 pathways gave 1340 mAh g^{-1} at 4 mg cm^{-2} and 0.1C with 89% retention after 100 cycles; at 8 mg cm^{-2}, the areal capacity reached 9.2 mAh cm^{-2} [18]. Residual chemistry and added electrolyte mass remain energy-density penalties. Operando tomography further indicates that such pathways should be assessed by through-thickness reaction uniformity, not endpoint capacity alone [6].

3.2.3. Coordinating anode deformation, electrolyte thickness, and pressure

At the anode, deformable lithium-storage structures can accommodate stripping deformation and homogenize current. The 80LiB/Ag@C design illustrates this physical function, but its 60-cycle evidence and inactive B/Ag mass constrain practical interpretation [16].

Reducing electrolyte thickness lowers both areal resistance and inactive mass. A Li_6PS_5Cl–carboxylated nitrile butadiene rubber (XNBR) separator thinner than 50 μm, used with an in situ polymerized lithium bis(fluorosulfonyl)imide–polydioxolane (LiFSI–PDOL) catholyte, enabled more than 50 cycles at 30 °C under relatively low stack pressure (<1 MPa) [19]. A cathode-supported approximately 100 μm Li_3PS_4/Kevlar electrolyte reported 370.6 Wh kg^{-1} at the cell-component level, excluding current collectors [20]. Thin layers, however, do not by themselves prevent lithium penetration through pre-existing defects.

Pressure must be matched to current and microstructure. In-containing cathodes formed InS/In_2S_3 at S/SSE interfaces, while capacity in the same system increased from 810 mA h g^{-1} at 1 MPa to 1198 mAh g^{-1} at 7 MPa (28 °C, 0.1C) [21]. These concurrent observations do not establish that the phases alone caused the pressure response. Separate studies show that excessive pressure can reduce

DOI: 10.54254/2755-2721/2026.36782

the current sustainable before lithium penetration, whereas lower pressure can suppress crack propagation [7, 8].

Fair comparison therefore requires the capacity basis (sulfur, lithium sulfide, composite cathode, or full cell) to be reported together with active-material loading, areal capacity, and current density or C-rate (current normalized to the theoretical one-hour capacity). Temperature and externally applied stack pressure should be stated alongside SSE chemistry and thickness, anode type, and lithium inventory. Where available, electrolyte-to-sulfur (E/S) and negative-to-positive (N/P) capacity ratios should also be reported, while charge arising from mediators or redox-active electrolytes should be separated from sulfur-conversion capacity through complementary chemical, imaging, and mechanical evidence.

4. Conclusion

A proposed coupled-failure framework links interfacial chemistry, transport, and mechanics. Evidence across separate studies is consistent with mutual reinforcement among these processes, but direct operando validation of the complete feedback loop remains limited; mechanistic claims should therefore distinguish observed links from inferred ones. An emerging design principle is to preserve selective interfacial chemistry, continuous ionic/electronic pathways, and sustainable mechanical contact. Strategies should be judged by whether they sustain all three during conversion and lithium cycling, not by a single high gravimetric capacity. Evidence-normalized evaluation requires transparent capacity bases, complete operating and cell-architecture details, and explicit accounting of inactive mass and non-sulfur charge contributions. Cross-validated full-cell data should establish whether an improvement persists at relevant areal loading with finite lithium.

References

[1] Liang, F., Wang, S., Liang, Q., Zhong, A., Yang, C., Qian, J., Song, H., & Chen, R. (2024). Insight into all-solid-state Li–S batteries: Challenges, advances, and engineering design. *Advanced Energy Materials, 14*, 2401959. https://doi.org/10.1002/aenm.202401959.

[2] Liu, T., Liu, R., Lu, C., & Song, W. (2025). Progress and prospects of inorganic solid-state electrolyte-based all-solid-state Li–S batteries. *Advanced Sustainable Systems, 9*, 2400555. https://doi.org/10.1002/adsu.202400555.

[3] Cao, D., Sun, X., Li, F., Bak, S.-M., Ji, T., Geiwitz, M., Burch, K. S., Du, Y., Yang, G., & Zhu, H. (2023). Understanding electrochemical reaction mechanisms of sulfur in all-solid-state batteries through operando and theoretical studies. *Angewandte Chemie International Edition, 62*, e202302363. https://doi.org/10.1002/anie.202302363.

[4] Ohno, S., Rosenbach, C., Dewald, G. F., Janek, J., & Zeier, W. G. (2021). Linking solid electrolyte degradation to charge carrier transport in the thiophosphate-based composite cathode toward solid-state lithium–sulfur batteries. *Advanced Functional Materials, 31*, 2010620. https://doi.org/10.1002/adfm.202010620.

[5] Fan, B., Guan, Z., Wu, L., Zhang, S., Tan, M., Luo, Z., Zhang, X., Ma, H., & Xue, B. (2023). Particle size control of cathode components for high-performance all-solid-state lithium–sulfur batteries. *Journal of the American Ceramic Society, 106*, 5781–5794. https://doi.org/10.1111/jace.19220.

[6] Kimura, Y., Tanaka, M., Kawasaki, S., Yanagihara, S., Huebner, J., Ishiguro, N., Nakamura, T., Sekizawa, O., Nitta, K., Uchimoto, Y., Amezawa, K., & Ohno, S. (2025). Unraveling asymmetric macroscopic reaction dynamics in solid-state Li–S batteries during charge–discharge cycles: Visualizing ionic transport limitations with operando X-ray computed tomography. *Advanced Energy Materials, 15*, e03863. https://doi.org/10.1002/aenm.202503863.

[7] Ning, Z., Li, G., Melvin, D. L. R., Chen, Y., Bu, J., Spencer-Jolly, D., Liu, J., Hu, B., Gao, X., Perera, J., Gong, C., Pu, S. D., Zhang, S., Liu, B., Hartley, G. O., Bodey, A. J., Todd, R. I., Grant, P. S., Armstrong, D. E. J., Marrow, T. J., Monroe, C. W., Bruce, P. G. (2023). Dendrite initiation and propagation in lithium metal solid-state batteries. *Nature, 618*, 287–293. https://doi.org/10.1038/s41586-023-05970-4.

[8] Wang, Y., Liu, T., Kumar, J. (2020). Effect of pressure on lithium metal deposition and stripping against sulfide-based solid electrolytes. *ACS Applied Materials & Interfaces, 12*, 34771–34776.

DOI: 10.54254/2755-2721/2026.36782

https://doi.org/10.1021/acsami.0c06201.
[9] Fan, J., Sun, W., Fu, Y., Guo, W. (2024). Activation of Li2S cathode by an organoselenide salt mediator for all-solid-state lithium–sulfur batteries. *Advanced Functional Materials, 34*, 2407166. https://doi.org/10.1002/adfm.202407166.
[10] Kwok, C. Y., Xu, S., Kochetkov, I., Zhou, L., Nazar, L. F. (2023). High-performance all-solid-state Li2S batteries using an interfacial redox mediator. *Energy & Environmental Science, 16*, 610–618. https://doi.org/10.1039/D2EE03297J.
[11] Fujita, Y., Ding, J., Kowada, H., Mori, S., Motohashi, K., Sakuda, A., Hayashi, A. (2025). Electrode/electrolyte interphase formation by lithium iodide in a Li2S-based positive electrode for all-solid-state batteries. *ACS Applied Energy Materials, 8*, 2192–2199. https://doi.org/10.1021/acsaem.4c02731.
[12] Song, H., Münch, K., Liu, X., Shen, K., Zhang, R., Weintraut, T., Yusim, Y., Jiang, D., Hong, X., Meng, J., Liu, Y., He, M., Li, Y., Henkel, P., Brezesinski, T., Janek, J., Pang, Q. (2025). All-solid-state Li–S batteries with fast solid–solid sulfur reaction. *Nature, 637*, 846–853. https://doi.org/10.1038/s41586-024-08298-9.
[13] Kim, H., Choi, H.-N., Hwang, J.-Y., Yoon, C. S., & Sun, Y.-K. (2023). Tailoring the interface between sulfur and sulfide solid electrolyte for high-areal-capacity all-solid-state lithium–sulfur batteries. *ACS Energy Letters, 8*, 3971–3979. https://doi.org/10.1021/acsenergylett.3c01473.
[14] Yu, Z., Singh, B., Yu, Y., & Nazar, L. F. (2025). Suppressing argyrodite oxidation by tuning the host structure for high-areal-capacity all-solid-state lithium–sulfur batteries. *Nature Materials, 24*, 1082–1090. https://doi.org/10.1038/s41563-025-02238-2.
[15] Wu, X., Pan, H., Zhang, M., Zhong, H., Zhang, Z., Li, W., Sun, X., Mu, X., Tang, S., He, P., & Zhou, H. (2024). Integrating lithium sulfide as a single ionic conductor interphase for stable all-solid-state lithium–sulfur batteries. *Advanced Science, 11*, 2308604. https://doi.org/10.1002/advs.202308604.
[16] Chen, Z., Liang, Z., Zhong, H., Su, Y., Wang, K., & Yang, Y. (2022). Bulk/interfacial synergetic approaches enable the stable anode for high energy density all-solid-state lithium–sulfur batteries. *ACS Energy Letters, 7*, 2761–2770. https://doi.org/10.1021/acsenergylett.2c01334.
[17] Yue, J., Huang, Y., Liu, S., Chen, J., Han, F., & Wang, C. (2020). Rational designed mixed-conductive sulfur cathodes for all-solid-state lithium batteries. *ACS Applied Materials & Interfaces, 12*, 36066–36071. https://doi.org/10.1021/acsami.0c08564.
[18] Su, Y., Ren, S., Lin, Q., Su, Y., Lin, Y., Jiang, W., & Zhang, Y. (2025). In situ solid electrolyte ionic pathway formation in high sulfur loading cathodes for high-performance all-solid-state lithium–sulfur batteries. *Advanced Energy Materials, 15*, 2500363. https://doi.org/10.1002/aenm.202500363.
[19] Kim, S., Chart, Y. A., Narayanan, S., & Pasta, M. (2022). Thin solid electrolyte separators for solid-state lithium–sulfur batteries. *Nano Letters, 22*, 10176–10183. https://doi.org/10.1021/acs.nanolett.2c04216.
[20] Xu, R., Yue, J., Liu, S., Tu, J., Han, F., Liu, P., & Wang, C. (2019). Cathode-supported all-solid-state lithium–sulfur batteries with high cell-level energy density. *ACS Energy Letters, 4*, 1073–1079. https://doi.org/10.1021/acsenergylett.9b00430.
[21] Chen, P., Qu, H., Zheng, D., Zhang, X., & Qu, D. (2025). Long cycle stability of all-solid-state lithium-sulfur batteries at low pressure and ambient temperature: Addressing contact and diffusion kinetics. *Advanced Functional Materials, 35*, 2423633. https://doi.org/10.1002/adfm.202423633.